Molecular Therapy
Oncology
Original Article

The reovirus variant RP116 is oncolytic in immunocompetent models and generates reduced neutralizing antibodies to Type 3 Dearing

Ki-Hoon Song,[1] Xiao Xiang,[2,3,7] So Hyun Lee,[1] Jong Kyu Woo,[1] Gansukh Enkhtaivan,[1] Carlos Rios Giraldo,[2,3] You-Rim Lee,[1] Yeo Jin Jeong,[1] Salar Pashangzadeh,[2,3] Negar Sharifi,[2,3] An-Dao Yang,[2,3] Huy-Dung Hoang,[2,3] Nam-Hyuk Cho,[5,6] Yeon-Sook Lee,[1] Dong Guk Park,[1,4] and Tommy Alain[2,3]

[1]ViroCure, #502, Ace TwinTower 1, 285 Digital-ro, Guro-gu, Seoul 08381, Republic of Korea; [2]Children's Hospital of Eastern Ontario Research Institute, Department of Biochemistry, Microbiology and Immunology, University of Ottawa, Ottawa, ON, Canada; [3]Centre for Infection, Immunity and Inflammation, Faculty of Medicine, University of Ottawa, Ottawa, ON, Canada; [4]Department of Surgery, Dankook University Hospital, Cheonan 31116, Republic of Korea; [5]Department of Microbiology and Immunology, College of Medicine, Seoul National University, Seoul 03080, Republic of Korea; [6]Seoul National University Bundang Hospital, Seongnam, Gyeonggi-do 13620, Republic of Korea

The mammalian reovirus Type 3 Dearing (T3D) is a naturally occurring oncolytic virus. We previously identified a T3D variant isolated from persistently infected cancer cells that has a premature stop codon mutation in the *S1* gene, generating a truncated σ1-attachment protein that lacks the globular head. We now report on the molecular characterization of this variant, named RP116, and assess its antitumor potential in human cancer cells and syngeneic mouse models. RP116 replicates efficiently in several cancer cell lines, shows reduced dependency for the JAM-A receptor, significantly decreases tumor growth in syngeneic models when injected either intratumorally or intravenously, and generates long-term cures and immune memory in combination with checkpoint inhibitors. Finally, we demonstrate that RP116 infection in mice leads to reduced production of neutralizing antibodies directed against reovirus T3D, preserving the efficacy of subsequent reovirus treatment. These results establish the value of developing RP116 as an additional oncolytic reovirus platform.

INTRODUCTION

Reoviruses are non-enveloped double-stranded RNA viruses that predominantly target the respiratory and gastrointestinal tracts of humans, causing mostly benign or asymptomatic infections.[1] Reoviruses have been widely studied in laboratory settings as models of viral propagation and tissue distribution, cell replication, and host immune responses, and within the past 20 years have been extensively investigated for their natural oncolytic potential against various cancer types. There are four main mammalian reovirus serotypes, Type 1 Lang (T1L), Type 2 Jones (T2J), Type 3 Dearing (T3D), and Type 4 Ndelle (T4N), which are strains defined primarily by their differences in the *S1* gene encoding for the viral attachment protein σ1.[2] σ1 is the reovirus protein whose sequence varies the most among strains and is the main target of neutralizing host immune responses in mammals.[3–6] Importantly, isolated monoclonal antibodies that neutralize viral infection are often directed against the protruding globular head of σ1 and are serotype specific.[2,7–10]

The reoviral protein σ1 mediates viral binding to the host cell using mainly the junctional adhesion molecule-A (JAM-A) receptor and cell surface carbohydrates.[11–13] The JAM-A-binding site, located within the globular head domain of σ1, is found conserved among all serotypes.[14] In addition, reoviruses can engage a range of sialic acid glycans, the integrin β1 and/or the neuronal receptor NgR1, within domains of σ1 or σ3 to bind and attach to host cells.[15,16] Prior to entry into the host cytoplasm where the virus replicates, the capsid of reoviruses must undergo proteolytic disassembly into intermediate subviral particles often mediated by cathepsin and other proteases within the endosomal pathway.[17] While the known serotypes may differ in sites of tissue replication and spread, studies on the anticancer and antitumor immune properties of reoviruses have thus far focused on the T3D strain.[18–23]

While being primarily cytolytic, exposure of reoviruses to cells *in vitro* can occasionally induce persistent infections, whereby the virus and cells mutate to establish a long-term infection characterized by secretion of viral progeny that are continuously re-infecting proliferating

Received 4 April 2024; accepted 28 June 2024;
https://doi.org/10.1016/j.omton.2024.200846.

[7]Present address: Key Laboratory of Biorheological Science and Technology (Chongqing University), Ministry of Education, Chongqing 400045, China

Correspondence: Dong Guk Park, ViroCure, #502, Ace TwinTower 1, 285 Digital-ro, Guro-gu, Seoul 08381, Republic of Korea.
E-mail: dylan_park@virocure.net
Correspondence: Tommy Alain, Children's Hospital of Eastern Ontario Research Institute, Department of Biochemistry, Microbiology and Immunology, University of Ottawa, Ottawa, ON, Canada.
E-mail: tommy@arc.cheo.ca

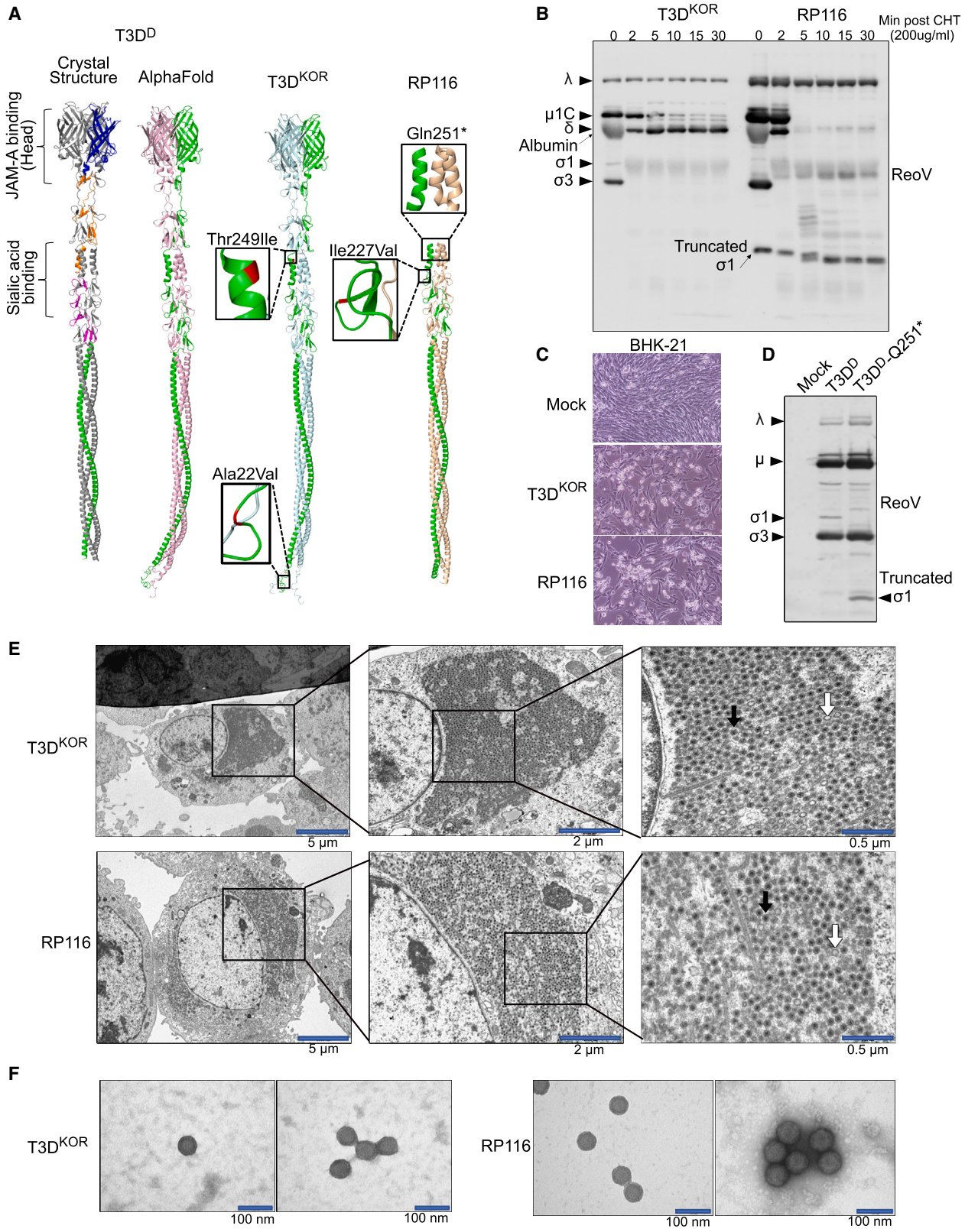

(legend on next page)

cells in the culture.[24–26] We previously described a reovirus variant isolated from persistently infected HT1080 human fibrosarcoma cells that exhibits a unique mutation at nucleotide position 763 (C>T) within the *S1* gene, resulting in a premature stop codon at amino acid 251.[26] This variant completely lacks the globular head of the σ1 attachment protein, but was found to still replicate efficiently in some cancer cell lines *in vitro*, and repressed tumor progression in human tumor xenografts grown in SCID/NOD mice.[26] Interestingly, this reovirus variant did not induce the myocarditis and necrotic morbidity associated with the "black foot" pathogenesis often seen with wild-type reovirus T3D administration to highly immunocompromised SCID/NOD mice,[27] and thus was initially classified as an attenuated reovirus.[26]

In this study, we further define the molecular characteristics of this unique truncated σ1 reovirus variant, named herein RP116, and address its broad direct cancer cell-lytic activity compared with a wild-type T3D reovirus (obtained from the Korea Biobank for Pathogenic Viruses [KBPV], hereby referred to as $T3D^{KOR}$). Characterization of oncolysis and markers attributed to reovirus-induced cell lysis in a panel of cancer cell lines derived from different tissues reveals a reduced requisite for the JAM-A receptor but a higher dependence of RP116 on sialic acid and integrin β1, as well as cathepsins and activated AKT signaling, as compared with $T3D^{KOR}$. Investigations into the synergistic potential of RP116 in combination with the immune checkpoint inhibitor (ICI) anti-PDL1 demonstrate robust cancer control and prolonged antitumor immune memory responses in syngeneic mouse models. Finally, we find reduced neutralizing antibodies against $T3D^{KOR}$ from mouse sera exposed to RP116, and we show that sequential therapeutic interventions of RP116 and $T3D^{KOR}$ improve tumor growth control as compared with sequential administration of the same virus. Altogether, our results establish the promise of developing RP116 as a novel cancer virotherapeutic.

RESULTS

Viral characterization of the RP116 variant

Reovirus infection of cell lines *in vitro* can occasionally generate a persistent infection. Several changes occurring within persistent viruses have been reported, particularly targeting the *S4* and *S1* genes encoding for the reovirus protein σ3 and σ1, respectively.[24,26,28,29] We previously isolated a unique reovirus variant from a persistently infected HT1080 human fibrosarcoma cell line. At the time, sequencing of the *S4* and *S1* genes revealed specific mutations including a C to T mutation within the *S1* gene at nucleotide position 763, leading to a change in amino acid Q251 to a stop codon (Q251*)[26] (Figure 1A). Despite this premature stop codon in σ1, the isolated virus was able to bind, infect, and replicate in a few tested cell lines and in tumor tissue *in vivo* from xenografts of HCT116 and HT1080 grown in SCID/NOD mice.[26]

We characterize here the molecular changes within the reovirus variant, RP116, that remained stable and infectious over time, having now been propagated over numerous (>20) passages in BHK21 and other cell types. Compared with reovirus T3D (GenBank accession number in materials and methods, also referred to as $T3D^{D}$ for Dermody laboratory[30,31]), and a reovirus T3D obtained from the KBPV ($T3D^{KOR}$), several missense and synonymous mutations were identified in most viral RP116 genes (Figures 1A, S1A–S1C; Table 1). In addition to the stop codon mutation in the *S1* gene, changes within the *S4*, *M3*, *M1*, and *L1* genes likely contribute to the infectivity, stability, and unique characteristics of this variant. For instance, sensitivity to chymotrypsin was assessed and RP116 particles showed accelerated proteolytic processing compared with reovirus $T3D^{KOR}$, as evidenced by a more rapid degradation of the viral protein μ1C and δ, and σ3 from the particle (Figure 1B). Of note, the truncated version of σ1 can be detected by western blotting and appears also to be partially cleaved during chymotrypsin treatment. Despite this increased proteolytic sensitivity, cytopathic effects induced by RP116 are similar to $T3D^{KOR}$ in BHK-21 cells (Figure 1C). Furthermore, a recombinant $T3D^{D}$ reovirus bearing only the premature stop codon mutation in the *S1* gene (referred to here as $T3D^{D-}$Q251*) was also able to be rescued and propagated over 10 times showing stability and infectivity similar to a recombinant $T3D^{D}$ (Figures 1D and S1D–S1F). To address whether RP116 infection may result in higher defective particles due to a truncated form of σ1, we performed transmission electron microscopy on $T3D^{KOR}$- and RP116-infected cells and purified particles. Viral factory production and particle size and shape appeared similar within BHK-21 cells between the two reoviruses (Figures 1E and 1F). These data confirm that RP116, and a $T3D^{D-}$Q251* recombinant virus, can be stable and replication-competent reovirus variants.

RP116 demonstrates oncolytic potential against various cancer cell types

The reovirus variant RP116 was previously reported to replicate in HT1080 fibrosarcoma cells and HCT116 colon carcinoma cells, and

Figure 1. RP116 exhibits accelerated proteolytic disassembly but similar viral particle size and shape to $T3D^{KOR}$

(A) Alpha Fold 2 prediction and Pymol visualization of σ1 trimer of reovirus $T3D^{D}$ (GenBank Accession: EF494435-44), $T3D^{KOR}$, and RP116. The crystal structure of $T3D^{D}$ σ1 trimer was used as structural reference. The σ1 monomer and the differences in amino acids are highlighted. (B) Representative western blotting shows accelerated proteolytic disassembly of purified particles of RP116 compared with $T3D^{KOR}$ after chymotrypsin treatment. (C) Representative brightfield microscopic images show similar level of cytopathic effect in BHK-21 cells after infection by $T3D^{KOR}$ or RP116. (D) $T3D^{D}$ carrying the characteristic Q251* mutation in σ1 can be rescued from the reverse genetic system. The total cell lysates from L929 cells 72 h after reoviral infection was analyzed by western blotting. The representative western blot shows detection of the truncated σ1 specifically in the $T3D^{D}$-Q251*-infected cells. (E) Scanning electron micrographs (SEM) and magnified views of the reoviral factory in the perinuclear area. Both $T3D^{KOR}$ and RP116 were assembled in the reoviral factory where genome containing complete viral particles (black arrows) and defective viral particles with hollow core (white arrow) can be observed from both variants. Bar, 5, 2, or 0.5 μm as indicated. (F) Representative SEM images show that both $T3D^{KOR}$ and RP116 particles possess the typical icosahedral outer capsid, and the two variants are similar in size. Bar, 100 nm.

Table 1. Changes found in RP116

		RP116		$T3D^{KOR}$		$T3D^{D}$	
Segment	Nucleotide position	Codon	Amino acid	Codon	Amino acid	Codon	Amino acid
L1	1220	aCt	Thr	aTt	Ile	aTt	Ile
	2959	Ctg	Leu	Atg	Met	Atg	Met
	3159	agA	Arg	agC	Ser	agC	Ser
	3167	aGc	Ser	aGc	Ser	aAc	Asn
	3628	Gaa	Glu	Aaa	Lys	Aaa	Lys
L2	1524	gAg	Glu	gAg	Glu	gGg	Gly
	1538	Cgg	Arg	Ggg	Gly	Ggg	Gly
	2900	Gtg	Val	Atg	Met	Atg	Met
	3807	aTa	Ile	aCa	Thr	aCa	Thr
L3	60	gTc	Val	gGc	Gly	gGc	Gly
	170	Cac	His	Tac	Tyr	Tac	Tyr
	453	cGg	Arg	cAg	Gln	cAg	Gln
	1512	aGc	Ser	aGc	Ser	aTc	Ile
	2569	caT	His	caG	Gln	caG	Gln
M1	134	Aac	Asn	Gac	Asp	Gac	Asp
	462	cGa	Arg	cAa	Gln	cAa	Gln
	635	Ccg	Pro	Ccg	Pro	Tcg	Ser
	1038	cAa	Gln	cAa	Gln	cGa	Arg
	1595	Tct	Ser	Gct	Ala	Gct	Ala
M2	248	gaC	Asp	gaA	Glu	gaA	Glu
	943	gCg	Ala	gTg	Val	gCg	Ala
	1329	Aac	Asn	Gac	Asp	Gac	Asp
	1960	gCg	Ala	gTg	Val	gTg	Val
M3	556	Gaa	Glu	Gaa	Glu	Aaa	Lys
	1450	Ctc	Leu	Atc	Ile	Atc	Ile
	1987	Gcc	Ala	Acc	Thr	Acc	Thr
	2132	gTt	Val	g(T/C)t	Val/Ala	gCt	Ala
	2138	gAt	Asp	gGt	Gly	gGt	Gly
S1	77	gCa	Ala	gTa	Val	gTa	Val
	691	Gta	Val	Ata	Ile	Ata	Ile
	758	aCt	Thr	aTt	Ile	aCt	Thr
	763	Taa	STOP	Caa	Gln	Caa	Gln
	1234	Gcg	Ala	Gcg	Ala	Acg	Thr
S2	167	aAg	Lys	aGg	Arg	aGg	Arg
S4	222	Gag	Glu	Aag	Lys	Aag	Lys
	429	Cgg	Arg	Tgg	Trp	Tgg	Trp
	562	tTc	Phe	tCc	Ser	tCc	Ser
	624, 625	AAg	Lys	g(A/G)g	Glu/Gly	GGg	Gly
	719	gaT	Asp	gaG	Glu	gaG	Glu
	784	cTc	Leu	cAc	His	cAc	His

to induce tumor regression of these human xenografts grown in SCID/NOD mice *in vivo*.[26] To investigate the extent by which RP116 is cytolytic against a broad panel of cancer cells, and to begin to address potential biomarkers that could mediate anticancer activity, cell viability assays were performed on a panel of 50 distinct cell lines comprising eight tumor types. To compare the anticancer

activity of RP116 and T3D^{KOR}, viral cytotoxicity was measured over a range of multiplicity of infection (MOI) based on total viral particle (VP) numbers. Experimental results showed that the IC_{50} (half-maximal inhibitory concentration) value for each cancer cell infected by RP116 or T3D^{KOR} varied between cancer types (Figures 2A and S2A–S2C; Table 2). Melanoma cell lines were found to be the most sensitive while conversely, gastric cancer cell lines were the least responsive to both RP116 and T3D^{KOR} (Figure S2B). Interestingly, breast cancer cell lines showed greater sensitivity to T3D^{KOR} than RP116 (Figure S2C). On the other hand, osteosarcoma cell lines were highly resistant to T3D^{KOR} infection, while moderate cytolytic activities against these cell models were detected from RP116 infection (Figure S2D). Taken together, these results show a varying sensitivity between different cancer cell types to the reoviruses T3D^{KOR} and RP116.

To investigate differences in oncolysis mediated by T3D^{KOR} and RP116, we next assessed the basal levels of the candidate receptors sialic acid, JAM-A, integrin β1, and NgR1 (Figures 2B and S2E–S2G). As expected, carcinomas with high JAM-A expression such as breast, ovarian, and bladder cancers were positively and significantly correlated with cytolysis by T3D^{KOR}, as compared with cancer cells with modest JAM-A expression such as osteosarcoma. In contrast, RP116, which lacks the JAM-A binding motif within its truncated σ1, showed no significant correlation between anticancer activity and JAM-A expression. Moreover, the oncolytic activity of RP116 was not independently correlated with expression levels of sialic acid or integrin β1. However, since the initial binding of reovirus σ1 protein to cell surface sialic acid can alter integrin β1 interaction,[32] separating the panel of cell lines for sialic acid^{low}/integrin β1^{low} and sialic acid^{high}/integrin β1^{high} expression groups revealed that cells exhibiting high expression of both sialic acid and integrin β1 were significantly associated with RP116 cytolytic activity (Figure S2F). We next analyzed the basal expression levels of several genes that have previously been reported to modulate sensitivity to reoviral oncolysis: the tumor suppressors p53, ATM, and Rb, the innate immune defense genes; TLR3, PKR, IRF family, Type I and II interferons and JAK/STAT, and genes implicated in viral entry; Cathepsin B/L, phosphorylated AKT (pAKT), and pERK1/2 (Figures 2C, 2D, and S2H–S2J).[22,33–38] Our analyses show that only the expression levels of pAKT and Cathepsin B/L have a significant correlation with the anticancer activity of RP116, but not with that of T3D^{KOR} (Figure 2D). Altogether, these results suggest that RP116 is more dependent on elevated sialic acid and integrin β1 expression than JAM-A as compared with T3D^{KOR}. Furthermore, the infectivity of RP116 may benefit from higher pAKT signaling and Cathepsin B/L activity.

RP116 is efficacious in syngeneic models by intratumoral and intravenous administration, and generates long-term cures in combination with ICIs

Pre-clinical and clinical studies with reovirus have assessed both the intratumoral (IT) or intravenous (i.v.) routes of administration for cancer treatment.[39] Previously, RP116 was assessed and demonstrated to cause tumor regression when administered IT in human cancer xenografts grown in SCID/NOD mice.[25] To determine the efficacy of RP116 in more clinically relevant immunocompetent animal models, we compared two different doses of IT and i.v. RP116 treatments on the syngeneic murine B16F10 melanoma model. Mice bearing B16F10 melanoma subcutaneous tumors were treated twice on following days with either 1×10^8 or 1×10^9 $TCID_{50}$ of RP116, either IT or i.v. Tumor sizes were measured until the tumor burden of the control group reached the limit for euthanasia. All four RP116 treatments showed significant tumor growth control and the best response was observed in the group that received the higher IT doses (Figure 3A). We next tested if additional i.v. treatments of RP116 could improve tumor regression. In the same model, mice were treated i.v. with 1×10^9 $TCID_{50}$ of RP116 two or five times on consecutive following days. Multiple i.v. injections were found to significantly delay tumor growth compared to only two injections. (Figure 3B). RP116 treatment was well tolerated in both injection models as body weight changes were not detected even after multiple high dosages of RP116 (Figure S3A). While significant inhibition of tumor growth was observed, B16F10 tumors were not completely eradicated by RP116 virotherapy alone and ultimately grew. Viral infection can activate Type I interferon (IFN) signaling and the expression of PDL1 on cancer cells.[40] Since overexpression of PDL1 on the surface of tumor cells can inhibit the activation of cytotoxic T cells, we expected that synergistic anticancer effects could be induced by subsequent administrations of ICIs such as anti-PDL1 antibodies.[41] In a repeated experiment of IT-administered RP116, follow-up therapy with anti-PDL1 antibodies showed dramatic improvement in tumor regression and prolonged mouse survival (Figures 3C and 3D).

These results prompted us to investigate the therapeutic effects of RP116 in combination with anti-PDL1 antibody therapy using two syngeneic mouse tumor models, namely B16F10 melanoma and EMT-6 breast cancer. We first measured PDL1 expression on the surface of B16F10 and EMT6 cells by flow cytometry. While B16F10 melanoma cells expressed PDL1 at a relatively high level, EMT-6 breast cancer cells showed only basal level of expression (Figure S3B). However, infection with RP116-induced PDL1 levels in both cell types and the induction fold was considerably higher with EMT-6 cells (Figure S3B). To assess the therapeutic effect of combining RP116 with ICIs, mice bearing either B16F10 or EMT-6 tumors were administered RP116 twice consecutively (on days 0, 1) and anti-PDL1 every 3 days (from day 0 for a total number of six administrations). In B16F10 melanoma, RP116 monotherapy showed similar level of tumor growth control compared with anti-PDL1 antibody monotherapy, with a 76% and 79% average tumor growth inhibition, respectively (Figures 3E and S3C). However, the combination therapy resulted in three (of 12) long-term survivors (Figure 3F). With the EMT-6 breast cancer model, we found that anti-PDL1 antibody monotherapy failed to control tumor growth, but RP116 monotherapy was effective, showing an average of 60% tumor growth inhibition (Figures 3G and S3D). Notably, in early phase of treatment, the combination therapy presented similar tumor growth inhibition to the

Table 2. List of cell lines

No.	Cancer type	Cell line	IC_{50} value (MOI, VP) of $T3D^{KOR}$	IC_{50} value (MOI, VP) of RP116	Sialic acids (MFI)	JAM-A (MFI)	ITGb1	CTSB	CTSL	NgR1	pAKT	pERK	TLR3
1	Bladder	253J/BV	59.67	16.36	1070	1262	0.49	10.59	6.03	9.09	21.16	3.45	1.71
2	Bladder	T24	273.90	27.12	1621	284	0.73	8.72	1.80	5.11	20.97	3.85	0.97
3	Bladder	5637	24.40	96.40	1263	2150	1.31	11.95	8.02	18.66	5.34	0.68	1.74
4	Bladder	J82	80.58	106.30	1225	591	1.32	11.93	5.35	1.94	25.11	3.34	0.98
5	Bladder	HT1376	45.95	821.30	1334	3431	2.20	6.65	11.58	49.70	6.20	1.08	0.85
6	Bladder	22Rv1	1.03	6463.00	263	264	0.00	0.01	0.81	18.42	3.84	3.56	5.29
7	Bladder	RT4	10178.00	25648.00	984	2502	0.24	9.50	2.34	20.13	1.51	0.73	0.90
8	Breast	T47D	1.12	703.10	717	4482	1.57	6.91	0.56	8.02	2.37	3.73	2.10
9	Breast	MCF-7	266.60	3758.00	590	2450	0.56	0.96	1.07	4.78	1.08	3.97	2.15
10	Breast	BT-20	3.19	6556.00	1686	2942	1.92	0.51	0.45	6.70	15.41	1.73	2.67
11	Breast	MDA-MB-231	2105.00	7401.00	1954	321	1.78	1.66	0.58	0.67	3.27	8.31	2.46
12	Breast	MDA-MB-453	284.70	35491.00	659	2131	0.65	0.84	0.08	15.70	2.70	2.40	3.35
13	Cervix	HeLa	94.05	18.86	2227	240	**1.00**[a]	**1.00**[a]	**1.00**[a]	**1.00**[a]	**1.00**[a]	**1.00**[a]	**1.00**[a]
14	Colorectal	HCT116	5.53	473.50	1043	1410	0.59	9.79	3.32	21.46	1.42	3.98	4.28
15	Colorectal	LOVO	8.01	536.40	975	1377	0.61	5.61	2.21	28.41	1.01	3.85	5.75
16	Colorectal	DLD-1	1036.00	21556.00	582	1144	0.32	7.99	2.74	29.15	1.56	0.96	3.13
17	Colorectal	HCT15	3662.00	N/A	367	947	0.31	11.65	3.04	29.39	1.31	1.18	2.83
18	Colorectal	HT29	3491.00	N/A	1006	2372	0.77	17.59	0.95	39.35	0.87	1.80	2.61
19	Gastric	MKN28	523.20	1653.00	1243	2907	0.00	0.14	3.31	22.97	18.16	4.12	3.35
20	Gastric	AGS	12176.00	29130.00	685	1258	0.00	0.19	0.04	111.83	6.98	3.99	13.25
21	Gastric	SNU668	9471.00	81209.00	1220	276	5.06	13.83	4.31	11.40	1.69	3.70	1.82
22	Gastric	KATOIII	6635.00	N/A	1405	1382	0.00	0.17	0.03	65.13	2.46	4.11	3.39
23	Gastric	MKN45	27467.00	N/A	1616	2515	0.00	0.06	0.35	5.04	2.73	1.75	3.42
24	Gastric	NCIN87	10922.00	N/A	1160	2418	0.01	0.40	1.55	119.90	6.65	7.60	3.88
25	Glioma	U87MG	102.60	47.40	1903	607	3.50	6.45	4.07	1.33	16.94	3.78	2.47
26	Glioma	SNU489	160.40	441.80	2155	393	5.06	14.99	4.31	3.18	11.33	1.58	2.32
27	Glioma	U373MG	3588.00	675.00	1173	262	3.16	14.19	4.94	0.96	16.18	1.58	2.48
28	Glioma	A172	1325.00	1630.00	1623	281	9.42	43.53	7.43	21.90	11.48	5.15	2.43
29	Glioma	SNU466	1325.00	1630.00	1817	581	2.46	28.76	8.46	5.30	18.41	1.58	2.56
30	Glioma	T98G	6532.00	2242.00	1732	208	1.32	6.42	1.19	5.16	10.11	1.65	2.43
31	Glioma	SNU201	491.40	7875.00	1482	790	1.87	60.66	29.58	3.80	6.78	1.03	1.99
32	Melanoma	WM-266-4	0.23	3.36	1310	516	2.95	26.09	2.16	8.89	23.86	7.68	2.53
33	Melanoma	A375	1.19	3.46	1051	212	0.85	9.43	4.89	2.13	7.21	7.29	2.47
34	Melanoma	HS294T	16.94	4.54	968	498	2.52	15.84	8.51	38.81	11.23	3.54	2.40
35	Melanoma	SKMEL-28	0.65	5.64	1024	944	2.55	181.27	18.12	58.86	10.08	7.25	3.16

(*Continued on next page*)

Table 2. ***Continued***

No.	Cancer type	Cell line	IC_{50} value (MOI, VP) of $T3D^{KOR}$	IC_{50} value (MOI, VP) of RP116	Sialic acids (MFI)	JAM-A (MFI)	ITGb1	CTSB	CTSL	NgR1	pAKT	pERK	TLR3
36	Melanoma	A431	139.70	308.50	2231	4031	2.80	6.49	2.54	22.94	2.78	1.04	2.29
37	Melanoma	SKMEL-3	11.94	329.30	528	208	1.09	17.76	10.15	22.70	5.04	3.25	2.72
38	Colon	CCD-18Co	4186.00	85.58	1743	240	0.01	5.07	44.07	0.72	11.99	3.58	0.20
39	Skin	HS27	N/A	1669.00	1214	166	9.51	26.64	3.16	0.60	4.59	1.79	1.58
40	Osteosarcoma	Saos-2	N/A	389.00	981	172	1.46	10.44	6.68	4.56	9.03	0.60	4.23
41	Osteosarcoma	Saos-LM2	N/A	744.60	1109	226	1.09	8.27	8.59	5.00	10.87	0.74	3.14
42	Osteosarcoma	U2OS	N/A	1065.00	759	135	4.14	10.98	2.11	32.41	9.24	1.88	2.10
43	Osteosarcoma	G-292	N/A	1688.00	649	150	1.93	30.81	3.88	0.78	3.71	9.17	1.19
44	Osteosarcoma	HOS	4189.00	1765.00	523	198	1.06	0.76	0.50	2.86	10.08	5.97	1.80
45	Osteosarcoma	MG-63	N/A	5893.00	748	156	3.10	76.27	10.54	25.22	10.55	1.99	1.39
46	Ovarian	SNU840	23.32	29.57	2534	2638	0.40	9.01	2.84	14.79	21.65	2.00	1.22
47	Ovarian	OVCAR-3	36.96	34.66	715	1430	0.67	17.78	3.25	31.97	2.01	3.00	14.04
48	Ovarian	SKOV-3	370.50	52.45	1388	384	1.80	41.69	15.71	59.75	12.67	2.46	1.26
49	Ovarian	SNU8	75.53	401.80	2598	2441	2.13	55.53	2.54	12.38	3.97	1.81	2.65
50	Ovarian	Caov-4	6.90	856.30	1690	1324	6.33	73.34	3.74	102.07	3.46	2.75	2.71

[a]Normalized based on gene expression levels in HeLa cells.

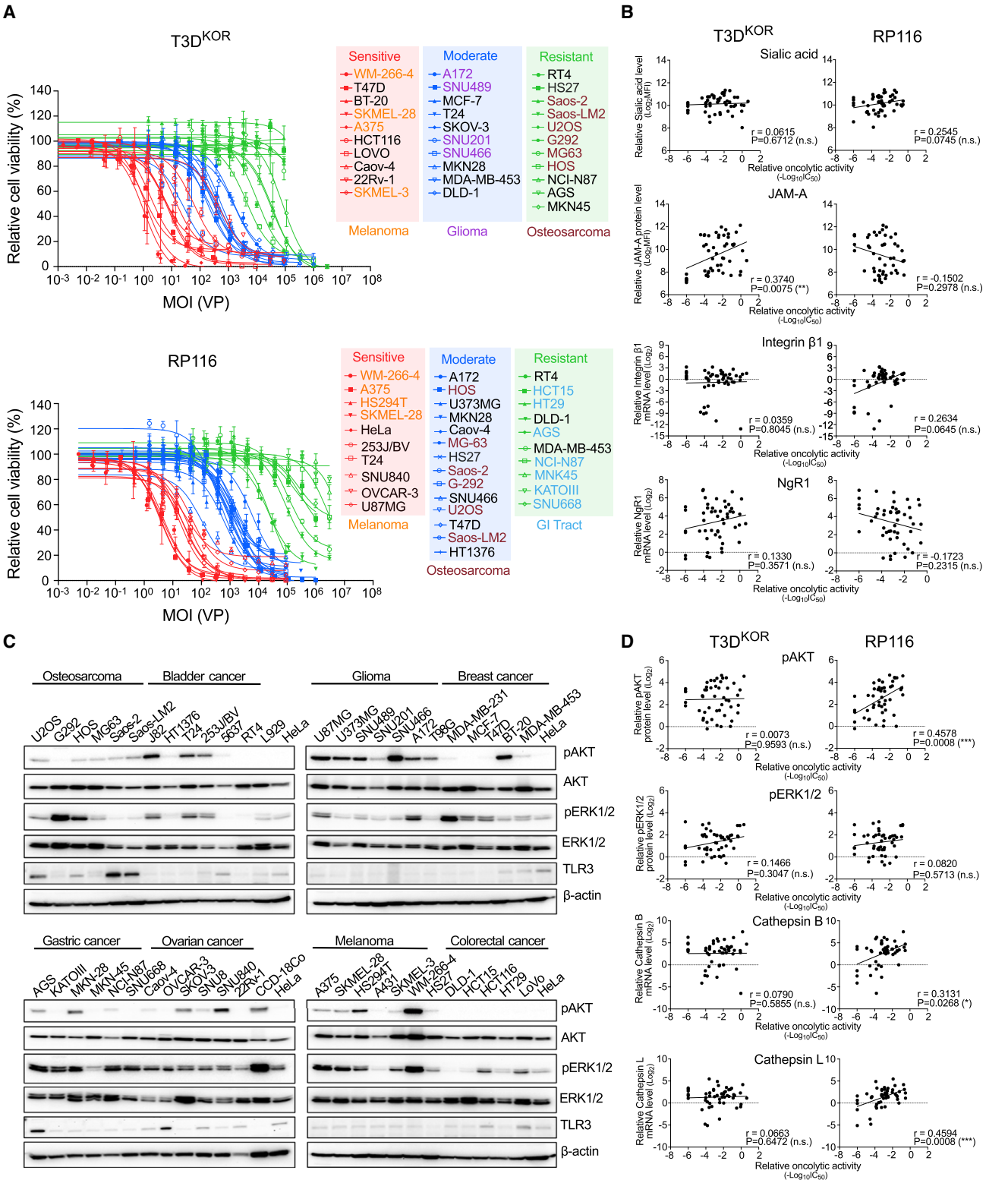

(legend on next page)

RP116 monotherapy group, but ultimately combining RP116 with anti-PDL1 antibodies led to significant improvement in anticancer effect, resulting in 67% (6 of 9) complete cures as compared with 17% (2 of 12) with RP116 treatment alone (Figure 3H). These findings demonstrate the robust viral immunotherapeutic effects of RP116.

RP116 and anti-PDL1 combination treatment stimulates immune anticancer memory

As RP116 monotherapy and the combined administration of RP116 with anti-PDL1 antibody treatment in the EMT6 model resulted in long-term surviving mice (complete responders [CR], $n = 2$ for the RP116 monotherapy group and $n = 6$ for the RP116+anti-PDL1 group), we designed follow-up studies to assess anticancer immune memory (Figure 4A). Four months (110 days) after the initial treatment administration, EMT6 cells were subcutaneously re-injected into the flanks of mice where the primary tumors had been eradicated. Tumor formation was monitored and compared with age-matched naive mice. During follow-up, we observed tumor recurrence in two mice, one from the RP116 monotherapy group (1 of 2) and the other from the combined therapy group (1 of 6). Thus, the final tumor-free mice in the EMT6 model was 75% (6 of 8), while none of the mice in the control group ($n = 10$) survived past 40 days (Figures 4B, 4C, and S4A). A second rechallenge was performed on the remaining tumor-free survivors ($n = 6$). For this second rechallenge experiment, 156 days post the initial treatment administration, EMT6 cells were injected into the caudal vein of mice to induce lung metastasis. During the incubation period, weight loss and breathing difficulties were observed in the naive age-matched control group ($n = 10$), but no abnormalities were observed in the CR group (Figure S4B). Twenty-five days after this second EMT-6 cell injection, lung metastasis was evaluated by lung nodule counts. There were no lung nodules observed in the CR mice group (0 of 6), whereas several lung nodules were observed from all (10 of 10) of the age-matched control group (Figure 4D). These results show that upon complete remission of the primary tumor from RP116 or its combination with ICIs, long-term immune memory from future tumor rechallenge can be established. These results also confirm the therapeutic potential of RP116-based immunotherapy to control primary tumors and prevent recurrence or metastasis.

To assess the long-term antitumor immunity against EMT6 cancer cells in further detail, splenocytes from the survivors of the recurrence and metastasis study were isolated and analyzed. First, establishment of EMT6-specific antitumor immunity was confirmed using ELISpot test comparing EMT-6 cells with two other murine cancer cell types, CT26 and Renca. Each cancer cell line was pretreated with mitomycin C for 24 h, and then co-cultured with splenocytes isolated from naive or CR mice. The interferon-γ secretion was observed specifically with EMT-6 cell co-culture (Figure 4E). We then confirmed that both central and effector memory formation of CD8+ and CD4+ T cells occurred in the mice of the CR mice group (Figure 4F). In particular, the difference of effector memory CD8+ T cells compared with the naive mouse groups may relate to the presence of large number of activated cytotoxic T lymphocytes. These results demonstrate that target-specific antitumor immunity is strongly established in mice whose cancer was eradicated through RP116 combination therapy.

RP116 immunogenically activates antigen-presenting cells

Having confirmed the antitumor immunotherapeutic potential of RP116 in combination with checkpoint inhibitors, we next wanted to compare the response of bone-marrow-derived dendritic cells (BMDCs) from mice upon exposure to RP116 or T3D^{KOR}. BMDCs were isolated and infected with the reoviruses and assessed for viral protein synthesis, viability, and induction of immunoregulatory cytokines through real-time qRT-PCR. We found that BMDCs can be infected, although poorly, by both T3D^{KOR} and RP116, as evidenced by the production of viral proteins in these cells (Figure 5A). However, limited toxicity was observed in these cells by both viruses even 7 days post infection (Figure 5B). Despite being similarly infected, we found that BMDCs treated with RP116 switched to promote a more immunogenic response compared with T3D^{KOR}. In particular, the expression of cytokines that control immunosuppression in the tumor microenvironment and cytokines that recruit immune cells into tumor tissues were increased in BMDCs infected with RP116 (Figure 5C). These results were also confirmed in experiments using the murine macrophage cell line RAW264.7 (Figures S5A and S5B). We also compared the cell surface protein expression levels of CD40, CD80, and CD86, other indicators of immune cell activation, which showed increased protein expression upon RP116 exposure as compared with T3D^{KOR} and/or uninfected controls (Figures 5D and S5C). In addition, RP116 treatment promoted higher MHC-II expression in RAW264.7 cells than T3D^{KOR} (Figure S5D). These findings suggest that RP116 infection induces a different immunogenic potential in immune cells compared with T3D^{KOR}.

Figure 2. Comparative analysis of the oncolytic activity of RP116 and T3D^{KOR} through screening of various cancer cell types

(A) Anticancer activity of T3D^{KOR} and RP116 in different types of cancer cells was used to determine IC_{50} values (Table 2). Using total viral particle (VP) numbers of each virus, T3D^{KOR} and RP116 were diluted to the indicated MOI. Relative oncolytic activities of both viruses are quantified by calculating the IC_{50} value. The relative susceptibility of cell lines against both viruses was depicted as scatterplots (top). Data are presented as mean ± SEM. (B) Correlation analysis between oncolytic activity of RP116 or T3D^{KOR} and basal levels of host cell receptors (sialic acids, JAM-A, *Integrin β1*, and *NgR1*). Cell surface levels of sialic acids and JAM-A were analyzed by flow cytometry using WGA lectin and antibody, respectively. Basal transcripts levels of *Integrin β1* and *NgR1* were analyzed by real-time qRT-PCR and normalized to *HPRT* expression. (C) Comparison of total and phosphorylated AKT and ERK1/2, and TLR3 protein levels in the panel of cell lines. The degree of activation and expression were detected by immunoblotting analysis using indicated specific antibodies. β-actin is shown as a loading control. (D) Correlation analysis between oncolytic activity of both viruses and levels of indicated candidate determinants. Activation levels of pAKT and pERK1/2 were analyzed by immunoblotting method (shown in C) and normalized using β-actin level for calculating relative values. Cathepsin B and L levels were analyzed by real-time qRT-PCR and normalized to *HPRT* expression. *p* values in (B) and (D) were calculated using two-tailed Spearman correlation analysis. Cell viability, western blot analysis, and real-time qRT-PCR data were a representative of two independent experiments, each with triplicate samples.

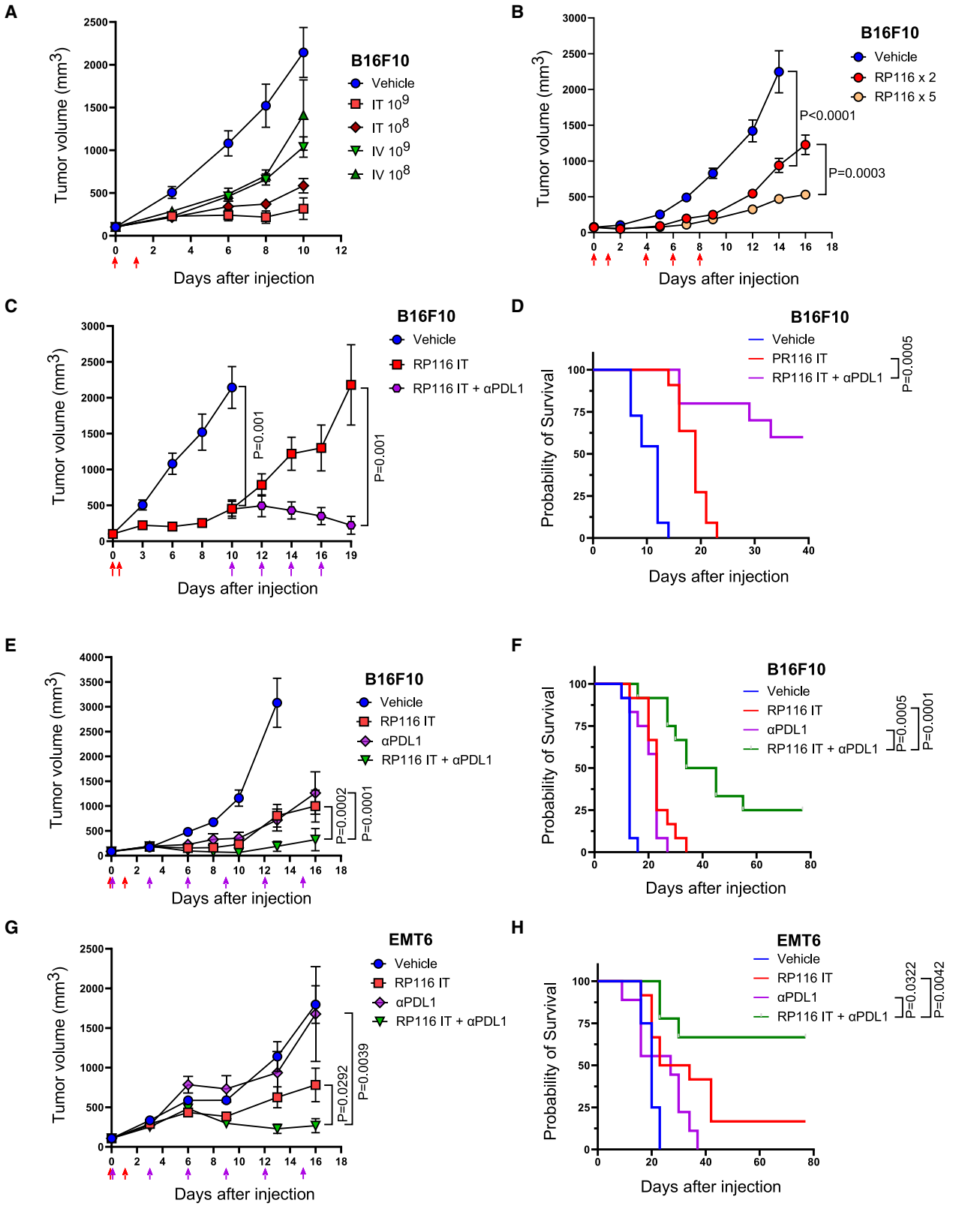

(legend on next page)

RP116 administration induces limited neutralizing antibody directed against T3D^{KOR} and tandem therapy improves tumor growth control

Neutralizing antibodies against oncolytic reovirus can prevent effective delivery and infection to tumor tissues and limit repetitive treatments.[42] The majority of neutralizing antibodies for reovirus are known to be directed against the globular head of the viral σ1 protein, which is absent in RP116. We hypothesized that sequential treatment of RP116 followed by T3D^{KOR} (or vice versa) would provide improved tumor growth control as compared with follow-up administration of the same virus. Using the B16F10 subcutaneous model, mice were either administered two i.v. infections (on subsequent days) of T3D^{KOR} or RP116, followed 7 days later with two injections of the same or the alternative virus. We found that sequential tandem therapy provided improved tumor growth control (Figures 6A–6C). We then compared characteristics of neutralizing antibodies generated by i.v. treatment of RP116 or T3D^{KOR}. The sera collected from RP116- or T3D^{KOR}- treated mice were used to determine neutralizing antibody titers against the two reoviruses. Interestingly, the neutralizing activity against T3D^{KOR} was lower in sera from RP116-treated mice (50% neutralization titer [NT_{50}] = 0.08) when compared with those from T3D^{KOR} solely injected mice (NT_{50} = 0.029), whereas neutralizing activity against RP116 was similar in sera from both mouse groups (0.005 vs. 0.007) (Figures 6D and 6E). These results showing reduced neutralization of T3D after initial exposure to RP116 suggest that RP116 could provide unhindered sequential therapeutic tandem interventions with an oncolytic reovirus T3D.

DISCUSSION

The reovirus Type 3 Dearing (T3D) is a naturally oncolytic virus that has been extensively investigated for its therapeutic potential against various cancer types through several clinical trials.[21,22,43] In this report, we present data on the RP116 variant of reovirus T3D, selected from persistently infected cancer cells, that display unique characteristics and immunotherapeutic potential. RP116 is a notable variant of reovirus as it harbors a stop codon mutation in the attachment σ1 protein of the virus at position amino acid Q251*. This mutation results in a truncated σ1 that lacks the globular head of the viral protein, which is involved in interaction with the JAM-A receptor. Interestingly, this mutation falls in the vicinity of a proteolytic cleavage site (Thr249) on σ1, and it was previously reported that such cleavage of the JAM-A-binding head domain of σ1 would result in diminished viral infectivity.[44,45] Nonetheless, we observed that RP116 was genetically stable over time and amplified efficiently in BHK-21 cells without reverting to wild-type T3D over multiple passages. Furthermore, RP116 was oncolytic against a variety of cancer cell models. While other mutations are present in several other viral genes within RP116, which could account for the stability and infectivity of this variant, we found that a recombinant T3D^{D-}Q251*, with no other mutational changes, could also be rescued and efficiently propagated. Thus, Q251* is a critical mutation that defines the characteristics of RP116, and our results demonstrate that variants of reoviruses lacking the globular head of their σ1 protein can exist and replicate in cell systems and tumor tissues.

We explored and compared here the cytotoxicity of RP116 and a T3D from the Korean Biobank (T3D^{KOR}) on a panel of well-established cancer cell lines. These analyses provided a range in sensitivity between the two viruses and allowed for the characterization of defined factors that had been reported to mediate selectivity to reovirus oncolysis. As expected, we confirmed that the T3D^{KOR} virus showed preferential cell killing for cells with a higher amount of JAM-A expression, the major receptor of reovirus. On the other hand, RP116, the variant lacking the JAM-A interaction motif, rather showed correlations with factors such as increased pAKT signaling and Cathepsin B/L expression. In addition, even though we found no significant correlation between anticancer activity and the expression levels of four known reovirus receptors when analyzed independently, a positive correlation was observed with RP116 in cells that displayed both high sialic acids and integrin β1 expression. As endocytosis of reovirus via sialic acids or integrin β1 is possible for cells with very low JAM-A expression, and that Cathepsin B/L and activated AKT signaling help with the processing of the viral capsid,[32,46] these molecular characteristics may cause different infection kinetics as observed among different cancer types. These analyses could also provide some selectivity in the type of malignancies that could be better targeted by RP116 compared with conventional T3D reovirus immunotherapy or vice versa. For instance, osteosarcoma cells with mesenchymal origin were much more resistant to T3D compared with RP116, while gastrointestinal-tract cancers, potentially with increased proteolytic activities, were refractory mainly to RP116. However, additional syngeneic cancer mouse models will be needed in the future to further validate the cancer tissue-dependent therapeutic potential of RP116 and T3D reovirus.

Figure 3. RP116 is efficacious in syngeneic models by IT and i.v. routes of administration and synergizes with immune checkpoint inhibition

(A–H) Cells were implanted subcutaneously (s.c.) in the right flank of C57BL/6 mice and treated with RP116 when tumor volume reached over 80 mm^3. The tumor volume, survival rate, and body weight were observed. Arrows represent time of treatment: red arrows (virus injection), purple arrows (anti-PDL1 administration). (A) Comparison between IT or i.v. administration of RP116 injection. Mice were injected with 1×10^8 and 1×10^9 $TCID_{50}$ of RP116 either IT or i.v. $n = 10$ (vehicle, IT 10^9, IT 10^8), 14 (i.v. 10^9) and 15 (i.v. 10^8). (B) Comparison of multiple i.v. injections of RP116. Mice were injected with 1×10^9 $TCID_{50}$ of RP116 by i.v. injection two or five times. $n = 9$ (vehicle), 8 (RP116 × 2), and 10 (RP116 × 5). (C) Combination therapy of RP116 with immune checkpoint inhibitors. Mice were treated twice with 1×10^8 $TCID_{50}$ of RP116 and then anti-PDL1 antibody treatment intraperitoneally starting from day 11. The combination of anti-PDL1 significantly reduced tumor growth. $n = 11$ (vehicle, RP116 IT) and 10 (RP116 IT + αPDL1). (D) Kaplan-Meier survival curves of mice injected with indicated treatments shown in (C). The p values in (B) and (C) were calculated using one-tailed Mann-Whitney test and (D) using a log rank test. (E–H) B16F10 (E) or EMT6 (F) cells were inoculated subcutaneously into immunocompetent mice and treated as indicated. Tumor growth inhibition was analyzed by measuring the tumor volume. $n = 12$ per group. Corresponding Kaplan-Meier survival curves for B16F10 (F) and EMT6 (H) treated groups. Animals were euthanized when tumors reached ∼2,000 mm^3 in size. p values: one-tailed Mann-Whitney test in (E) and (F) and a log rank test in (G) and (H). $^*p < 0.05$, $^{**}p < 0.01$, $^{***}p < 0.001$. Data are mean ± SEM.

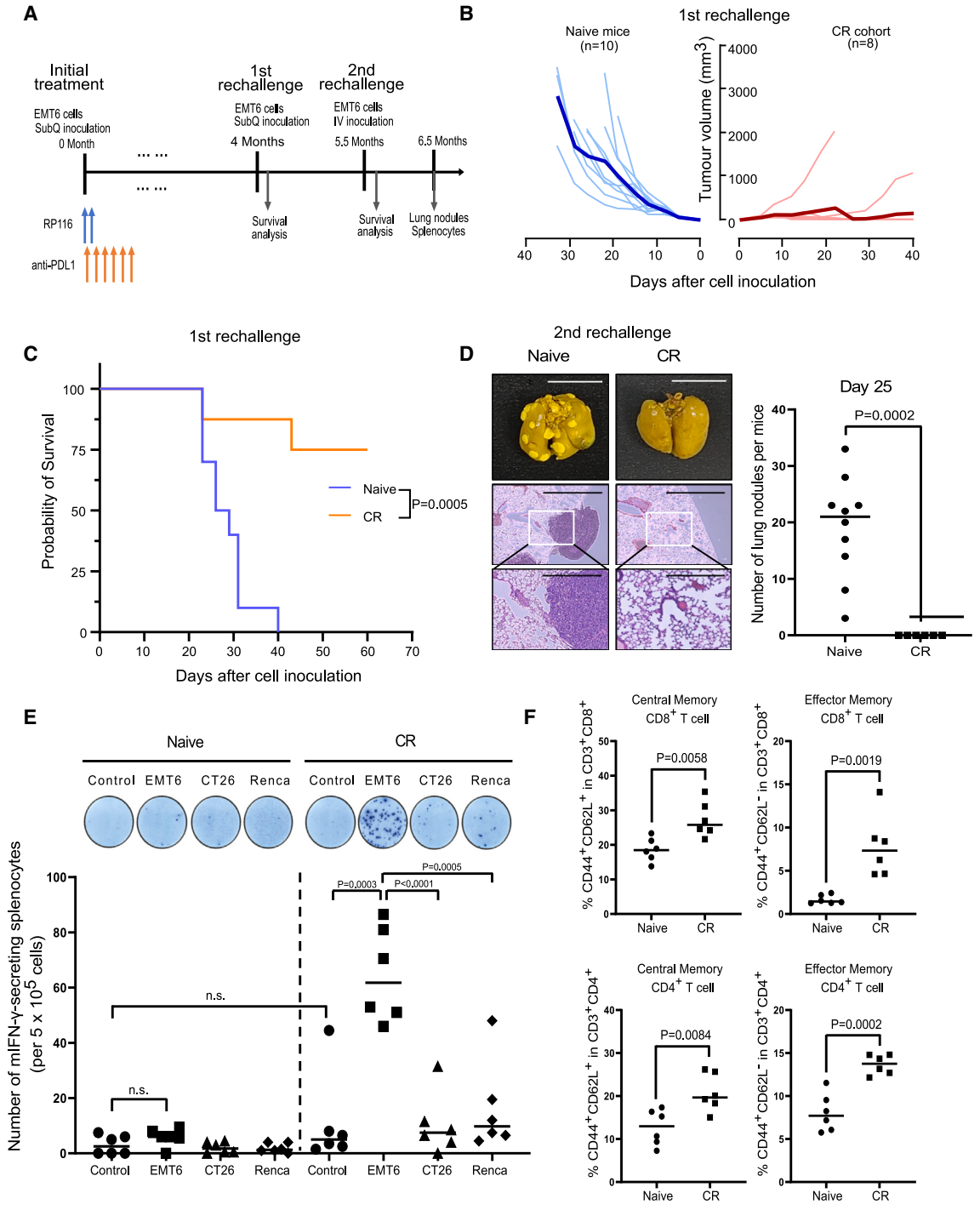

Figure 4. Combinatorial administration of RP116 and anti-PDL1 inhibits tumor recurrence and lung metastasis through the establishment of tumor-specific anticancer memory

(A) Outline of the RP116 and/or anti-PDL1 treatment regimen and rechallenge studies from experiment presented in Figures 3G and 3H. (B) First rechallenge study of mice that achieved complete regression against EMT6 tumors. Four months after RP116 and anti-PDL1 were administered, complete responders (CR) and age-matched treatment-naive mice were subcutaneously inoculated with EMT6 cells. n = 10 (naive) and n = 8 (CR). (C) Corresponding Kaplan-Meier survival plot of subcutaneously rechallenged mice from (B). (D) Second rechallenge study using experimental lung metastasis analysis. CR in first rechallenge study and age-matched naive mice were intravenously introduced with EMT6 cells. Left: Representative images of lungs fixed in Bouin's solution and histological staining (H&E) of lung sections. Scale bar, 10, 0.1,

(legend continued on next page)

Upon the original discovery and isolation of the RP116 variant, this virus was initially investigated for its oncolytic potential against two human xenograft models (HT1080 and HT29) in SCID/NOD mice.[26] RP116 intratumoral administration was successful in inducing the regression of these tumors; the variant also did not induce the myocarditis and necrotic morbidity often observed with reovirus T3D tumor infection in highly immunocompromised mice.[27] To better assess whether RP116 could have oncolytic and immunotherapeutic potential in immunocompetent animals, we treated two syngeneic mouse cancer models (B16F10 and EMT6) with RP116 either IT or i.v., which showed that this variant could provide robust tumor growth control. *In vitro* experiments also showed that PDL1 expression on the cell surface increased by RP116 treatment in both models, and as expected from these results, co-administration of RP116 with anti-PDL1 antibody therapy showed superior antitumor efficacy and even generated complete cures, particularly with the EMT6 model. Two rounds of consecutive rechallenge experiments were conducted with CRs, which confirmed the prolonged tumor-specific and antitumor memory by immune cells, including $CD8^+$ and $CD4^+$ T cells, that were acquired in the cured animals. Furthermore, we observed that RP116 treatment activates immune cells to express a higher amount of pro-innate and inflammatory cytokines. This could be a result of the difference in the infection kinetics between RP116 and $T3D^{KOR}$ as the detection of viral protein in BMDCs following RP116 infection was more delayed, potentially resulting in a moderate but more sustained immune cell activation. Furthermore, the mutations in addition to Q251* in RP116 may also have reshaped the antigenicity of the viral proteins leading to different immune responses.

Remarkably, treatment of RP116 generates reduced neutralizing antibodies against the reovirus $T3D^{KOR}$. This was anticipated as not only the globular head is the most immunogenic domain of reovirus, but it is also the major site responsible for mediating receptor-mediated viral entry. We found that the anti-sera generated by RP116 infection exerted poor levels of neutralization to $T3D^{KOR}$, likely from antibodies generated by RP116 viral proteins other than σ1. These results add to the current evidence that the σ1 globular head is both the most immunogenic and susceptible site for neutralizing antibodies. While the JAM-A binding globular head of σ1 has received the most attention as an immunogen, other findings, together with our current study, also suggest the existence of other neutralizing antibody-binding sites. For instance, Berkley et al. have shown that reovirus can be neutralized by both seral immunoglobulin (Ig)G and IgA antibodies, and that their electron micrographs of reoviral particles coated with anti-serum showed IgG bindings near the sialic acid binding region and on the viral capsid.[47] Although this is not definitive proof of other epitopes for neutralizing antibodies, their existence should not be dismissed. Moreover, in our study, we have demonstrated considerable neutralization of $T3D^{KOR}$ using the anti-sera from RP116. Given the lack of σ1 globular head, RP116 must have generated neutralizing antibodies that can recognize other epitopes. However, our data do not suggest the sialic acid binding region to be the dominant site for neutralizing antibodies due to lack of the effective cross-neutralization of RP116 by $T3D^{KOR}$ anti-serum. In other words, the sialic acid region-targeting neutralizing antibodies in the $T3D^{KOR}$ anti-serum must not be abundant since effective neutralization of this domain will completely prevent reoviral attachment.[45] Further studies are ongoing to assess the role of neutralizing antibodies and antibody functions in RP116-mediated oncolysis. More importantly, we found that tandem treatment with RP116 and $T3D^{KOR}$ improves tumor growth control, proposing that sequential therapeutic approaches could be designed when patients are to receive multiple doses of reovirus therapy.

This study provides the evaluation of a novel variant of the oncolytic reovirus T3D, RP116, characterized by a unique premature stop codon mutation in the σ1 attachment protein, that still provides robust immunotherapeutic efficacy when combined with ICIs. Additional development of RP116 for the treatment of specific cancer types and in combination with subsequent reovirus T3D treatment may result in improved tumor responses in patients.

MATERIALS AND METHODS

Mice and primary cell culture

Six-week-old female C57BL/6 and BALB/c mice were purchased from NARA-Biotech (Seoul, South Korea) and ORIENT BIO Inc. (Seoul, South Korea), respectively. Mouse were housed in an animal care facility at Virocure Inc. (Seoul, South Korea). All animal experiments were approved by the Institutional Animal Care and Use Committee (#VRC-2001) of Virocure Inc. and were carried out using approved protocols. The cultivation of mouse-derived BMDCs is succinctly detailed as follows: bone marrow cells were aspirated from the femurs and pelvic bones of mice using a syringe, followed by centrifugation to collect the isolated cells. Subsequently, these cells were cultured in a Petri dish with 20 ng/mL granulocyte-macrophage colony-stimulating factor (Sigma) in DMEM supplemented with 10% fetal bovine serum (FBS). The medium underwent three changes every 48 h, and following the final medium exchange, only the cells detached by pipetting were harvested for experimental use. Viability experiments for BMDCs included seeding the cultured cells into a 96-well plate, administering the virus at concentrations specified in the figure, introducing WST solution at different time points, and assessing cell viability through absorbance readings.

and 0.01 mm from top to bottom, respectively. Right: Number of lung nodules in naive (n = 10) or CR mice (n = 6). (E) ELISpot assay using splenocytes from naive mice or those from mice previously cured in second EMT6 rechallenge study. Splenocytes were stimulated with EMT6, CT26.WT, or Renca. Number of mice with IFN-γ-secreting splenocytes was quantified by counting positive spots. Top: Representative images of ELISpot analysis. (F) The populations of central or effector memory T cells were analyzed using flow cytometry. Splenocytes isolated from naive or CR mice were stained with anti-CD3, anti-CD8, anti-CD4, anti-CD44, and anti-CD62L antibodies. p values in (D), (E), and (F) were calculated using two-tailed unpaired Student's t test and (C) using a log rank test. $^*p < 0.05$, $^{**}p < 0.01$, $^{***}p < 0.001$; n.s., not significant.

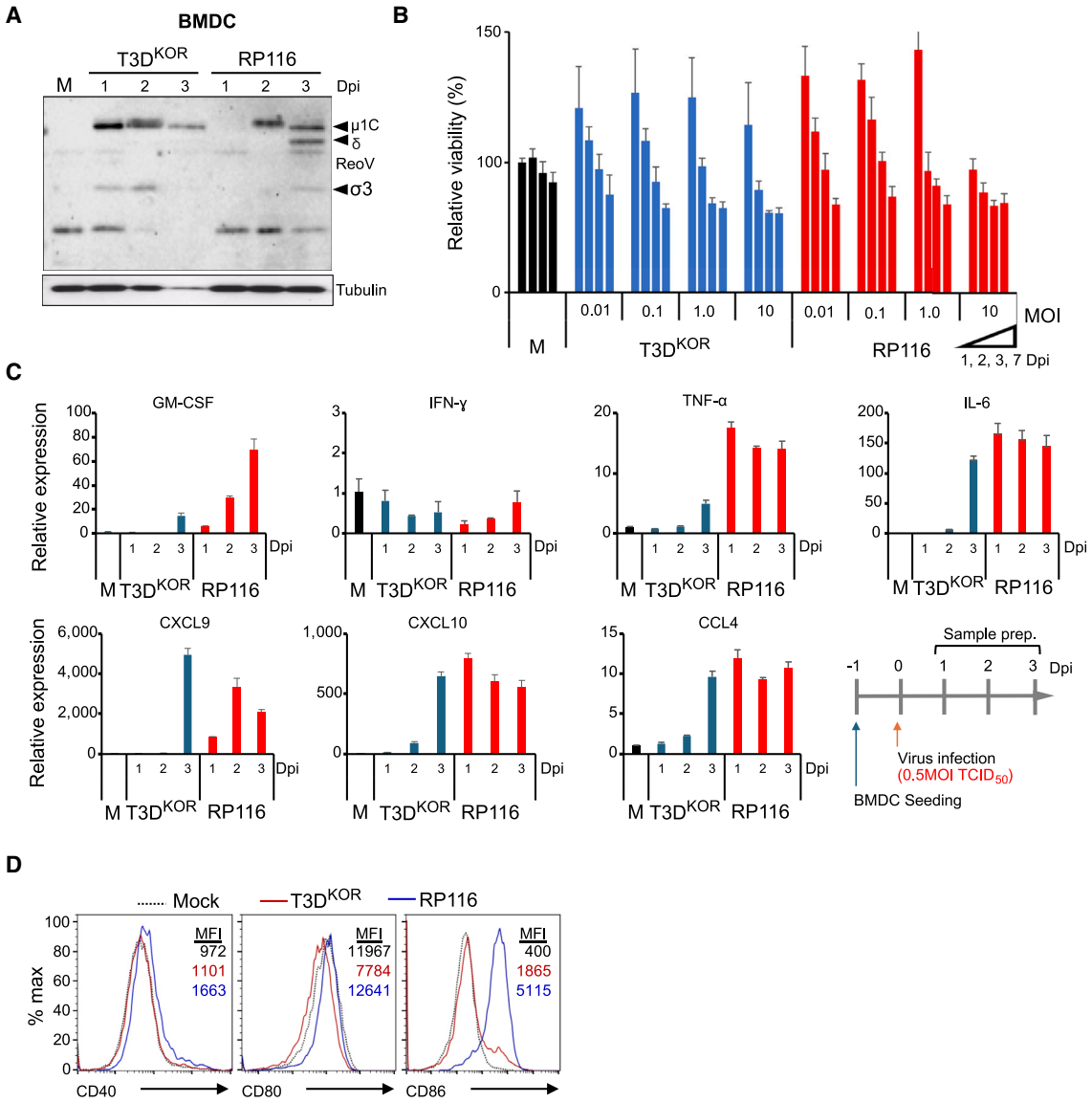

Figure 5. RP116 infection on bone marrow-derived cells alters cellular immune responses

(A) Bone marrow-derived cells (BMDCs) were infected with T3D^{KOR} or RP116 for 1, 2, and 3 days. Expression of viral proteins was assessed by immunoblot using polyclonal rabbit sera against reovirus. M, mock-infected. Tubulin was used as a loading control. (B) The viability of BMDCs following infection with either T3D^{KOR} or RP116 was assessed through the utilization of WST-1. (C) Total RNA was purified from BMDCs, and cytokine expression was determined using real-time qRT-PCR. (D) The cell activation markers of BMDCs infected with T3D^{KOR} or RP116 were analyzed using FACS. Results are presented as mean ± SD.

Syngeneic mouse tumor model

A total of 1×10^5 B16F10 cells in a 100-μL Matrigel (Corning) and PBS mixture (1:1), were implanted in the right flank of C57BL/6 mice by subcutaneous injection. Treatments started when the tumor volume reached over 80 mm^3. For the comparison between intratumoral (IT) or intravenous (i.v.) injection, mice were treated with 1×10^8 and 1×10^9 of the 50% of tissue culture infective dose ($TCID_{50}$) of RP116 by either IT or i.v. injection on day 0 and day 1. For multiple i.v. injections, 1×10^9 $TCID_{50}$ of RP116 was delivered two times (days 0 and 1) or five times (days 0, 1, 3, 5, and 7) by i.v. injection. For combination efficacy of RP116 with αPDL1 antibody (B7-H1, BioXCell, Lebanon, NH, USA), the 1×10^8 $TCID_{50}$ of RP116 was injected twice and 10 mg per kg (mpk) of αPDL1 antibody was injected four times. The tumor size was measured two or three times in a week using a caliper, and tumor volume was calculated by a modified ellipsoid formula as 0.5 × (Length × Width2).

Cell lines and culture conditions

Various cell lines, including breast cancer, colon cancer, stomach cancer, brain tumor, malignant skin cancer, bone cancer, ovarian cancer,

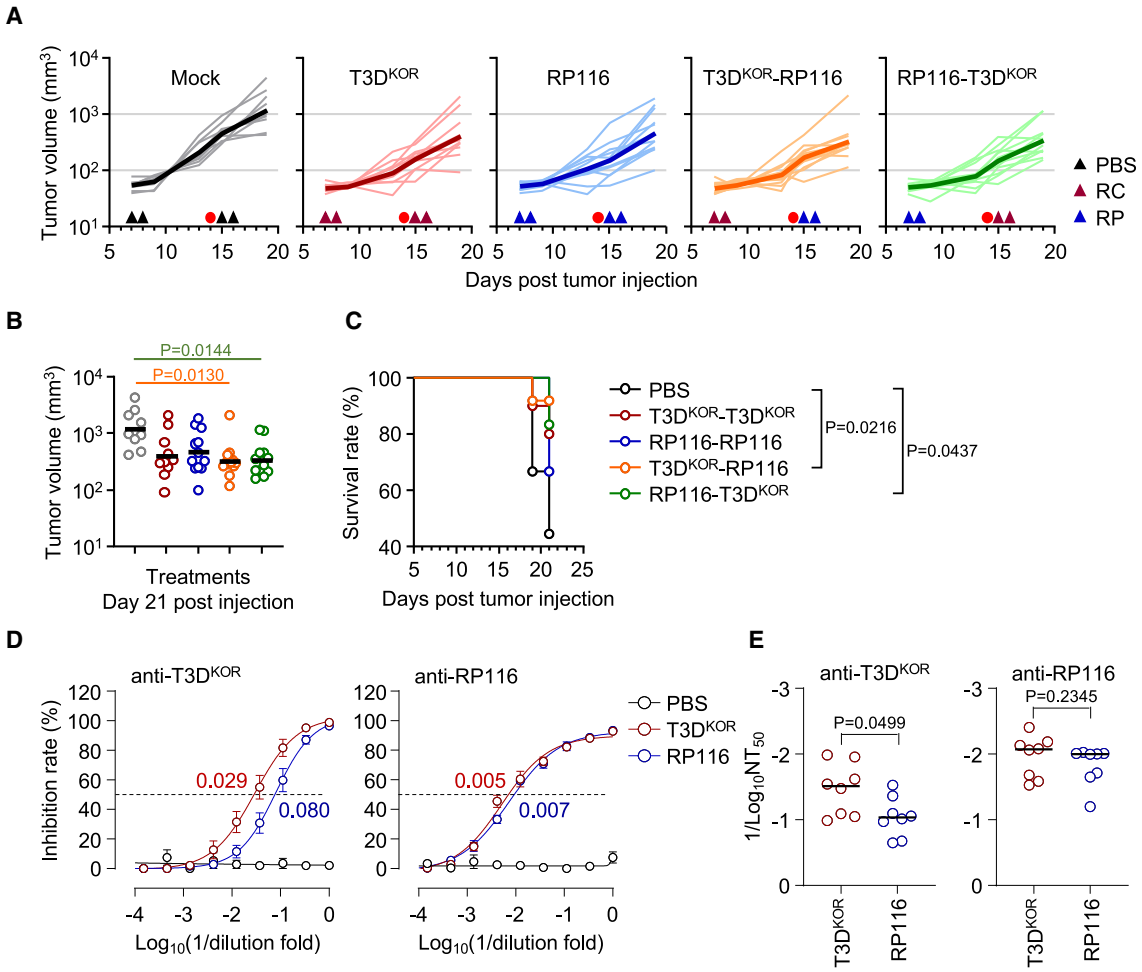

Figure 6. Neutralization activity of sera from tandem virotherapy

(A and B) Comparison of tumor growth in mice carrying B16F10 melanoma after combinatorial challenge of RP116 and T3D^{KOR}. Arrows represent time of treatments, red dots represent sera collection for neutralizing antibody assay. Thick lines in (A) are the mean tumor volume, which is quantified in (B). (C) Kaplan-Meier survival plot of challenged mice from experiment presented in (A). (D and E) Neutralizing antibody titers against the T3D^{KOR} (left panel) and RP116 (right panel) of sera collected from mice immunized with T3D^{KOR} (red) or RP116 (blue) at 7 days post-immunization. Fifty percent neutralizing antibody titers are colored accordingly. *p* values: one-tailed Mann-Whitney test, $^{**}p < 0.01$.

and human skin and colon fibroblast cell, HS27 and CCD-18Co cells, respectively, were obtained from ATCC (Manassas, VA) and Korea Cell Line Bank (Seoul, South Korea). RAW264.7 was purchased from Sigma-Aldrich (MA, USA). Bladder cancer cell lines 253J/BV, T24, 5637, J82, HT1376, 22Rv1, and RT4 were kindly provided by Dr. Duck Cho (Samsung Seoul Hospital, Seoul, South Korea). All cell lines were maintained in the appropriate medium specified by their suppliers while supplemented with 10% FBS without antibiotics except for RAW264.7 where an additional 1% penicillin/streptomycin was added and MB752/1, which was maintained in 15% FBS and 2 mM L-glutamine instead. All cell lines were incubated at 5% CO_2 and 37°C unless otherwise specified.

Oncolytic activity: IC_{50} value

The anticancer activity of T3D^{KOR} and RP116 was confirmed on a total of 50 different cell lines, including 48 cell lines of eight carcinomas and two normal cells. Approximately 4×10^3 cells were seeded in each well in a 96-well plate and allowed to adhere for 6 h. The cells were then infected by T3D^{KOR} and RP116 at a series of decreasing MOIs determined using VP standards. Three to 4 days post infection, the cells were incubated with 10 μL of E Z-CyTox (DoGenBio, Seoul, South Korea) for 1–3 h before being read on a microplate reader (Molecular Devices, San Jose, CA) with an absorbance spectrum of 450 nm. The value IC_{50} was calculated using the Prism program. The IC_{50} values for each of the 50 cell lines can be found in Table 1.

Quantitative real-time PCR (qRT-PCR)

Total RNA was isolated from each cell using Qiazol (Qiagen, Valencia, CA) and chloroform. A total of 200 ng RNA was used in the THUNDERBIRD one-step real-time qRT-PCR reaction according to the manufacturer's instructions (Toyobo, Osaka, Japan). Specific primers for *ITGB1*, *NGR1*, *CTSB*, *CTSL*, and *HPRT* genes were

analyzed on a real-time PCR machine, CFX96 (Biorad, Hercules, CA). The primer information for each gene is provided in Table S1. The ΔΔCt method was used to analyze the raw Ct values.

Western blot analysis

Cells in culture were washed using cold PBS and lysed with RIPA cell lysis buffer (Thermo Fisher Scientific) supplemented with protease inhibitor (Roche, Basel, Switzerland), which was then quantified using the BCA Protein assay kit (Sigma-Aldrich, Missouri, MO). The cell lysates were separated on 10% SDS-PAGE and then transferred onto a polyvinylidene difluoride (PVDF) membrane (Roche). The PVDF membrane was visualized using enhanced chemiluminescent (ECL) substrate (ThermoFisher Scientific, Waltham, MA) after being incubated with appropriate primary and secondary antibodies. Please refer to Table S2 for detailed information about each antibody used.

Flow cytometry

Flow cytometry assay was performed to confirm the basic expression levels of sialic acids and JAM-A present on the cell surface. Approximately, 0.2–1 $\times$ 10^6 cells were collected and stained using WGA (Vector Labs, Burlingame, CA) for sialic acid and anti-JAM-A (BioLegend, San Diego, CA) for JAM-A for 1 h at 4°C. For analysis of BMDC and RAW264.7 cells, harvested cells were stained with conjugated monoclonal antibodies against MHC-II, CD40, CD80, and CD86 (Invitrogen, Waltham, MA). The cells were then washed twice with cold PBS and submitted to flow cytometry analysis using Attune NxT cytometer (Thermo Fisher Scientific, Waltham, MA) and the results were analyzed by FlowJo software (BD, NJ). Please refer to Table S2 for detailed information about each antibody used.

Neutralizing anti-reovirus antibody assay

Serum samples collected from mice 14 days post reovirus infection were used to determine neutralizing antibody titers against reovirus. Briefly, serum samples were serially diluted at 3-fold (i.e., 1:1, 1:3, 1:9, 1:27, 1:81, 1:243) in DMEM in 96-well plates at a final volume of 50 μL. Then, 50 μL of $T3D^{KOR}$ or RP116 reovirus suspension containing 100 PFU was added to each well. The plate was gently agitated and incubated for 1 h at 37°C. After incubation, 100 μL of L929 cells (5.0×10^5 cells/mL) were added to each well and incubated for another 72 h. The wells were examined for the appearance of CPE, and the neutralizing antibody titers were calculated as the $\log_{10}$ of the reciprocal antibody dilution required for 50% neutralization of 100 PFU of reovirus. All tests were repeated independently at least twice.

Protein structure prediction and visualization

AlphaFold2 (version v2.2.3) was used to predict the structure of reoviral proteins from $T3D^D$, $T3D^{KOR}$, and RP116. The predicted protein structures were then visualized by PyMol (version 2.5.4.). To generate the complete crystal structure of σ1 from $T3D^D$, two existing crystal structures of σ1 (Protein DataBank [PDB] identifier: 6GAP and 3S6Y) were joined together using the "align" command in PyMol after removing amino acids beyond position 171 in 6GAP and amino acids before position 170 in 3S6Y. The crystal structures of all other reoviral proteins were retrieved from UNIPROT with their corresponding PDB identifiers listed below except for Mu2 and MuNS whose crystal structures were yet to be resolved at the time. GenBank accession numbers for the 10 genes of $T3D^D$ used as references are as follows: L1: EF494435.1, L2: EF494436.1, L3: EF494437.1, M1: EF494438.1, M2: EF494439.1, M3: EF494440.1, S1: EF494441.1, S2: EF494442.1, S3: EF494443.1, and S4: EF494444.1.

Statistical analysis

Unpaired two-tailed Student's t tests and analysis of variance followed by Tukey's or Bonferroni post hoc tests were used. Results are given as mean ± SD. Results with $p < 0.05$ were considered statistically significant. Each experiment was performed at least three times ($n \geq 3$). The exact number of times each experiment was performed is indicated in the figure legends. The individual data points are also displayed on the graphs. Correlation analysis was performed using Spearman's rank correlation test. Statistical significance was also calculated using the same program, and statistical significance was considered when the p value was <0.05.

DATA AND CODE AVAILABILITY

The data presented herein are available within the main text, figures, and tables of the manuscript and supplementary data files.

SUPPLEMENTAL INFORMATION

Supplemental information can be found online at https://doi.org/10.1016/j.omton.2024.200846.

ACKNOWLEDGMENTS

The authors wish to thank the late Dr. Manbok Kim for his dedication and unwavering enthusiasm in pursuing research to help patient care. This research was supported partly by a grant of the Korea Health Technology R&D Project through the Korea Health Industry Development Institute (KHIDI), funded by the Ministry of Health & Welfare, Republic of Korea (grant number: HV22C0009) to Y.-S.L., D.G.P., and N.-H.C. The work was also supported by the Technology Development Program (grant number: B200287) funded by the Ministry of SMEs and Startups (MSS, Republic of Korea). This work was partially supported also by a Terry Fox Research Institute New Project Grant, a Natural Sciences and Engineering Research Council of Canada (NSERC) Discovery grant, a Cancer Research Society grant, a Canadian Cancer Society Research Institute Innovation to Impact Grant (#706852) and Canadian Institute of Health Research (CIHR) bridge funding to T.A., H.-D.H., and X.X.

AUTHOR CONTRIBUTIONS

Conceptualization, K.-H.S., Y.-S.L., D.G.P., N.-H.C., and T.A.; methodology, K.-H.S., X.X., S.H.L., J.K.W., C.R.G., Y.-R.L., Y.J.J., A.-D.Y., H.-D.H., S.P., N.S., and G.E.; investigation, K.-H.S., X.X., S.H.L., and J.K.W.; writing—original draft preparation, K.-H.S., Y.-S.L., D.G.P., N.-H.C., X.X., and T.A.; writing—review and editing, K.-H.S., Y.-S.L., D.G.P., N.-H.C., T.A., H.-D.H., and X.X.; supervision, Y.-S.L., D.G.P, N.-H.C., and T.A. All authors have read and agreed to the published version of the manuscript.

DECLARATION OF INTERESTS

K.-H.S., S.H.L., J.K.W., Y.-R.L., and Y.J.J. are employees of the company Virocure Inc., which supported the current research on the RP116 reovirus. N.-H.C. and T.A. are acting scientific officers and consultants for Virocure Inc. Y.-S.L. was the chief technology officer and D.G.P. is the current chief executive officer at Virocure Inc.

REFERENCES

1. Tyler, K.L., Clarke, P., DeBiasi, R.L., Kominsky, D., and Poggioli, G.J. (2001). Reoviruses and the host cell. Trends Microbiol. *9*, 560–564. https://doi.org/10.1016/s0966-842x(01)02103-5.
2. Dietrich, M.H., Ogden, K.M., Katen, S.P., Reiss, K., Sutherland, D.M., Carnahan, R.H., Goff, M., Cooper, T., Dermody, T.S., and Stehle, T. (2017). Structural Insights into Reovirus σ1 Interactions with Two Neutralizing Antibodies. J. Virol. *91*, e01621-16. https://doi.org/10.1128/JVI.01621-16.
3. Duncan, R., Horne, D., Cashdollar, L.W., Joklik, W.K., and Lee, P.W. (1990). Identification of conserved domains in the cell attachment proteins of the three serotypes of reovirus. Virology *174*, 399–409. https://doi.org/10.1016/0042-6822(90)90093-7.
4. Nibert, M.L., Dermody, T.S., and Fields, B.N. (1990). Structure of the reovirus cell-attachment protein: a model for the domain organization of sigma 1. J. Virol. *64*, 2976–2989. https://doi.org/10.1128/JVI.64.6.2976-2989.1990.
5. Chappell, J.D., Prota, A.E., Dermody, T.S., and Stehle, T. (2002). Crystal structure of reovirus attachment protein sigma1 reveals evolutionary relationship to adenovirus fiber. EMBO J. *21*, 1–11. https://doi.org/10.1093/emboj/21.1.1.
6. Weiner, H.L., and Fields, B.N. (1977). Neutralization of reovirus: the gene responsible for the neutralization antigen. J. Exp. Med. *146*, 1305–1310. https://doi.org/10.1084/jem.146.5.1305.
7. Burstin, S.J., Spriggs, D.R., and Fields, B.N. (1982). Evidence for functional domains on the reovirus type 3 hemagglutinin. Virology *117*, 146–155. https://doi.org/10.1016/0042-6822(82)90514-1.
8. Tyler, K.L., Mann, M.A., Fields, B.N., and Virgin, H.W.t. (1993). Protective anti-reovirus monoclonal antibodies and their effects on viral pathogenesis. J. Virol. *67*, 3446–3453. https://doi.org/10.1128/JVI.67.6.3446-3453.1993.
9. Helander, A., Miller, C.L., Myers, K.S., Neutra, M.R., and Nibert, M.L. (2004). Protective immunoglobulin A and G antibodies bind to overlapping intersubunit epitopes in the head domain of type 1 reovirus adhesin sigma1. J. Virol. *78*, 10695–10705. https://doi.org/10.1128/JVI.78.19.10695-10705.2004.
10. Hutchings, A.B., Helander, A., Silvey, K.J., Chandran, K., Lucas, W.T., Nibert, M.L., and Neutra, M.R. (2004). Secretory immunoglobulin A antibodies against the sigma1 outer capsid protein of reovirus type 1 Lang prevent infection of mouse Peyer's patches. J. Virol. *78*, 947–957. https://doi.org/10.1128/jvi.78.2.947-957.2004.
11. Kirchner, E., Guglielmi, K.M., Strauss, H.M., Dermody, T.S., and Stehle, T. (2008). Structure of reovirus sigma1 in complex with its receptor junctional adhesion molecule-A. PLoS Pathog. *4*, e1000235. https://doi.org/10.1371/journal.ppat.1000235.
12. Reiss, K., Stencel, J.E., Liu, Y., Blaum, B.S., Reiter, D.M., Feizi, T., Dermody, T.S., and Stehle, T. (2012). The GM2 glycan serves as a functional coreceptor for serotype 1 reovirus. PLoS Pathog. *8*, e1003078. https://doi.org/10.1371/journal.ppat.1003078.
13. Gentsch, J.R., and Pacitti, A.F. (1987). Differential interaction of reovirus type 3 with sialylated receptor components on animal cells. Virology *161*, 245–248. https://doi.org/10.1016/0042-6822(87)90192-9.
14. Stettner, E., Dietrich, M.H., Reiss, K., Dermody, T.S., and Stehle, T. (2015). Structure of Serotype 1 Reovirus Attachment Protein σ1 in Complex with Junctional Adhesion Molecule A Reveals a Conserved Serotype-Independent Binding Epitope. J. Virol. *89*, 6136–6140. https://doi.org/10.1128/JVI.00433-15.
15. Sutherland, D.M., Strebl, M., Koehler, M., Welsh, O.L., Yu, X., Hu, L., Dos Santos Natividade, R., Knowlton, J.J., Taylor, G.M., Moreno, R.A., et al. (2023). NgR1 binding to reovirus reveals an unusual bivalent interaction and a new viral attachment protein. Proc. Natl. Acad. Sci. USA *120*, e2219404120. https://doi.org/10.1073/pnas.2219404120.
16. Reiter, D.M., Frierson, J.M., Halvorson, E.E., Kobayashi, T., Dermody, T.S., and Stehle, T. (2011). Crystal structure of reovirus attachment protein σ1 in complex with sialylated oligosaccharides. PLoS Pathog. *7*, e1002166. https://doi.org/10.1371/journal.ppat.1002166.
17. Alain, T., Kim, T.S., Lun, X., Liacini, A., Schiff, L.A., Senger, D.L., and Forsyth, P.A. (2007). Proteolytic disassembly is a critical determinant for reovirus oncolysis. Mol. Ther. *15*, 1512–1521. https://doi.org/10.1038/sj.mt.6300207.
18. Kauffman, R.S., Wolf, J.L., Finberg, R., Trier, J.S., and Fields, B.N. (1983). The sigma 1 protein determines the extent of spread of reovirus from the gastrointestinal tract of mice. Virology *124*, 403–410. https://doi.org/10.1016/0042-6822(83)90356-2.
19. Tyler, K.L., McPhee, D.A., and Fields, B.N. (1986). Distinct pathways of viral spread in the host determined by reovirus S1 gene segment. Science *233*, 770–774. https://doi.org/10.1126/science.3016895.
20. Danthi, P., Holm, G.H., Stehle, T., and Dermody, T.S. (2013). Reovirus receptors, cell entry, and proapoptotic signaling. Adv. Exp. Med. Biol. *790*, 42–71. https://doi.org/10.1007/978-1-4614-7651-1_3.
21. Mahalingam, D., Goel, S., Aparo, S., Patel Arora, S., Noronha, N., Tran, H., Chakrabarty, R., Selvaggi, G., Gutierrez, A., Coffey, M., et al. (2018). A Phase II Study of Pelareorep (REOLYSIN®) in Combination with Gemcitabine for Patients with Advanced Pancreatic Adenocarcinoma. Cancers *10*, 160. https://doi.org/10.3390/cancers10060160.
22. Muller, L., Berkeley, R., Barr, T., Ilett, E., and Errington-Mais, F. (2020). Past, Present and Future of Oncolytic Reovirus. Cancers *12*, 3219. https://doi.org/10.3390/cancers12113219.
23. Malhotra, J., and Kim, E.S. (2023). Oncolytic Viruses and Cancer Immunotherapy. Curr. Oncol. Rep. *25*, 19–28. https://doi.org/10.1007/s11912-022-01341-w.
24. Alain, T., Kim, M., Johnston, R.N., Urbanski, S., Kossakowska, A.E., Forsyth, P.A., and Lee, P.W. (2006). The oncolytic effect in vivo of reovirus on tumour cells that have survived reovirus cell killing in vitro. Br. J. Cancer *95*, 1020–1027. https://doi.org/10.1038/sj.bjc.6603363.
25. Kim, M., Chung, Y.H., and Johnston, R.N. (2007). Reovirus and tumor oncolysis. J. Microbiol. *45*, 187–192.
26. Kim, M., Garant, K.A., zur Nieden, N.I., Alain, T., Loken, S.D., Urbanski, S.J., Forsyth, P.A., Rancourt, D.E., Lee, P.W., and Johnston, R.N. (2011). Attenuated reovirus displays oncolysis with reduced host toxicity. Br. J. Cancer *104*, 290–299. https://doi.org/10.1038/sj.bjc.6606053.
27. Loken, S.D., Norman, K., Hirasawa, K., Nodwell, M., Lester, W.M., and Demetrick, D.J. (2004). Morbidity in immunosuppressed (SCID/NOD) mice treated with reovirus (dearing 3) as an anti-cancer biotherapeutic. Cancer Biol. Ther. *3*, 734–738. https://doi.org/10.4161/cbt.3.8.963.
28. Ahmed, R., and Fields, B.N. (1982). Role of the S4 gene in the establishment of persistent reovirus infection in L cells. Cell *28*, 605–612. https://doi.org/10.1016/0092-8674(82)90215-x.
29. Wetzel, J.D., Wilson, G.J., Baer, G.S., Dunnigan, L.R., Wright, J.P., Tang, D.S., and Dermody, T.S. (1997). Reovirus variants selected during persistent infections of L cells contain mutations in the viral S1 and S4 genes and are altered in viral disassembly. J. Virol. *71*, 1362–1369. https://doi.org/10.1128/JVI.71.2.1362-1369.1997.
30. Mohamed, A., Clements, D.R., Gujar, S.A., Lee, P.W., Smiley, J.R., and Shmulevitz, M. (2020). Single Amino Acid Differences between Closely Related Reovirus T3D Lab Strains Alter Oncolytic Potency In Vitro and In Vivo. J. Virol. *94*, e01688-19. https://doi.org/10.1128/JVI.01688-19.
31. Kobayashi, T., Antar, A.A., Boehme, K.W., Danthi, P., Eby, E.A., Guglielmi, K.M., Holm, G.H., Johnson, E.M., Maginnis, M.S., Naik, S., et al. (2007). A plasmid-based reverse genetics system for animal double-stranded RNA viruses. Cell Host Microbe *1*, 147–157. https://doi.org/10.1016/j.chom.2007.03.003.
32. Koehler, M., Petitjean, S.J.L., Yang, J., Aravamudhan, P., Somoulay, X., Lo Giudice, C., Poncin, M.A., Dumitru, A.C., Dermody, T.S., and Alsteens, D. (2021). Reovirus directly engages integrin to recruit clathrin for entry into host cells. Nat. Commun. *12*, 2149. https://doi.org/10.1038/s41467-021-22380-0.
33. Coffey, M.C., Strong, J.E., Forsyth, P.A., and Lee, P.W. (1998). Reovirus therapy of tumors with activated Ras pathway. Science *282*, 1332–1334. https://doi.org/10.1126/science.282.5392.1332.

34. Kim, M., Williamson, C.T., Prudhomme, J., Bebb, D.G., Riabowol, K., Lee, P.W., Lees-Miller, S.P., Mori, Y., Rahman, M.M., McFadden, G., and Johnston, R.N. (2010). The viral tropism of two distinct oncolytic viruses, reovirus and myxoma virus, is modulated by cellular tumor suppressor gene status. Oncogene *29*, 3990–3996. https://doi.org/10.1038/onc.2010.137.

35. Roth, A.N., Aravamudhan, P., Fernandez de Castro, I., Tenorio, R., Risco, C., and Dermody, T.S. (2021). Ins and Outs of Reovirus: Vesicular Trafficking in Viral Entry and Egress. Trends Microbiol. *29*, 363–375. https://doi.org/10.1016/j.tim.2020.09.004.

36. Phillips, M.B., Stuart, J.D., Rodriguez Stewart, R.M., Berry, J.T., Mainou, B.A., and Boehme, K.W. (2018). Current understanding of reovirus oncolysis mechanisms. Oncolytic Virother. *7*, 53–63. https://doi.org/10.2147/OV.S143808.

37. Alexopoulou, L., Holt, A.C., Medzhitov, R., and Flavell, R.A. (2001). Recognition of double-stranded RNA and activation of NF-kappaB by Toll-like receptor 3. Nature *413*, 732–738. https://doi.org/10.1038/35099560.

38. Nan, Y., Wu, C., and Zhang, Y.J. (2017). Interplay between Janus Kinase/Signal Transducer and Activator of Transcription Signaling Activated by Type I Interferons and Viral Antagonism. Front. Immunol. *8*, 1758. https://doi.org/10.3389/fimmu.2017.01758.

39. Macedo, N., Miller, D.M., Haq, R., and Kaufman, H.L. (2020). Clinical landscape of oncolytic virus research in 2020. J. Immunother. Cancer *8*, e001486. https://doi.org/10.1136/jitc-2020-001486.

40. Farrukh, H., El-Sayes, N., and Mossman, K. (2021). Mechanisms of PD-L1 Regulation in Malignant and Virus-Infected Cells. Int. J. Mol. Sci. *22*, 4893. https://doi.org/10.3390/ijms22094893.

41. Ren, Y., Miao, J.M., Wang, Y.Y., Fan, Z., Kong, X.B., Yang, L., and Cheng, G. (2022). Oncolytic viruses combined with immune checkpoint therapy for colorectal cancer is a promising treatment option. Front. Immunol. *13*, 961796. https://doi.org/10.3389/fimmu.2022.961796.

42. Groeneveldt, C., Kinderman, P., Griffioen, L., Rensing, O., Labrie, C., van den Wollenberg, D.J.M., Hoeben, R.C., Coffey, M., Loghmani, H., Verdegaal, E.M.E., et al. (2024). Neutralizing antibodies impair the oncolytic efficacy of reovirus but permit effective combination with T cell-based immunotherapies. Cancer Immunol. Res. *12*, 334–349. https://doi.org/10.1158/2326-6066.CIR-23-0480.

43. Chaurasiya, S., Fong, Y., and Warner, S.G. (2021). Oncolytic Virotherapy for Cancer: Clinical Experience. Biomedicines *9*, 419. https://doi.org/10.3390/biomedicines9040419.

44. Nibert, M.L., Chappell, J.D., and Dermody, T.S. (1995). Infectious subvirion particles of reovirus type 3 Dearing exhibit a loss in infectivity and contain a cleaved sigma 1 protein. J. Virol. *69*, 5057–5067. https://doi.org/10.1128/JVI.69.8.5057-5067.1995.

45. Fernandes, J.P., Cristi, F., Eaton, H.E., Chen, P., Haeflinger, S., Bernard, I., Hitt, M.M., and Shmulevitz, M. (2019). Breast Tumor-Associated Metalloproteases Restrict Reovirus Oncolysis by Cleaving the σ1 Cell Attachment Protein and Can Be Overcome by Mutation of σ1. J. Virol. *93*, e01380-19. https://doi.org/10.1128/JVI.01380-19.

46. Koehler, M., Aravamudhan, P., Guzman-Cardozo, C., Dumitru, A.C., Yang, J., Gargiulo, S., Soumillion, P., Dermody, T.S., and Alsteens, D. (2019). Glycan-mediated enhancement of reovirus receptor binding. Nat. Commun. *10*, 4460. https://doi.org/10.1038/s41467-019-12411-2.

47. Berkeley, R.A., Steele, L.P., Mulder, A.A., van den Wollenberg, D.J.M., Kottke, T.J., Thompson, J., Coffey, M., Hoeben, R.C., Vile, R.G., Melcher, A., and Ilett, E.J. (2018). Antibody-Neutralized Reovirus Is Effective in Oncolytic Virotherapy. Cancer Immunol. Res. *6*, 1161–1173. https://doi.org/10.1158/2326-6066.CIR-18-0309.